

# Volume Encoding Gaussians: Transfer-Function-Agnostic 3D Gaussians for Volume Rendering

Landon Dyken\*, Andres Sewell\*, Will Usher, Steve Petruzza, Sidharth Kumar

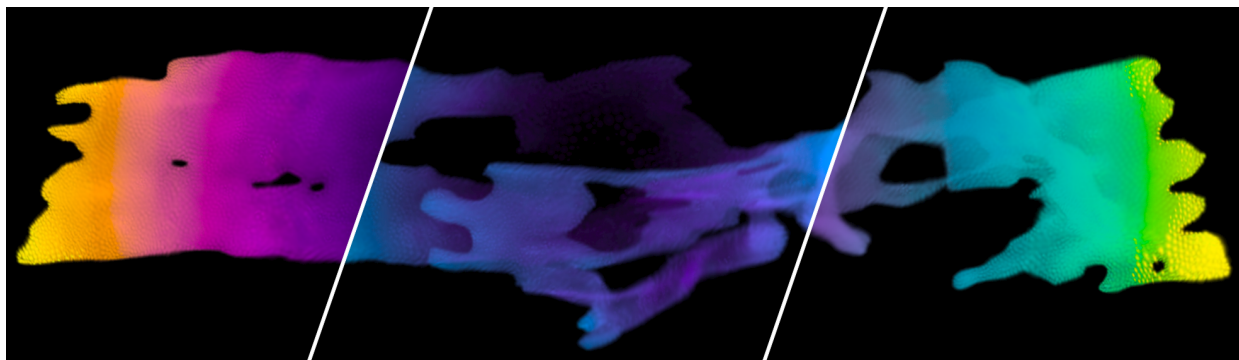


Fig. 1: Transfer-function-agnostic rendering with *Volume Encoding Gaussians (VEG)* on the RBL unstructured volume dataset. Unlike conventional 3D Gaussian Splatting methods that store view-dependent color and opacity for each Gaussian, VEG encodes only the underlying scalar field values, enabling real-time flexibility in choosing transfer functions. This design yields significant data compression (up to a  $3600\times$  ratio for massive datasets) for volume data, while retaining high visual fidelity for approximating volume rendering. Here, the same trained VEG model is rendered with three distinct colormaps: plasma (left), rainbow (middle), and viridis (right), all generated from the same representation without retraining. White lines indicate the boundaries between colormap transitions, demonstrating that transfer functions can be swapped while preserving structural detail. While this dataset cannot be interactively rendered using PyVista [35] or ParaView, our method is able to perform unstructured volume rendering of this dataset at  $> 500$  frames per second.

**Abstract**—While HPC resources are increasingly being used to produce adaptively refined or unstructured volume datasets, current research in applying machine learning-based representation to visualization has largely ignored this type of data. To address this, we introduce *Volume Encoding Gaussians (VEG)*, a novel 3D Gaussian-based representation for scientific volume visualization focused on unstructured volumes. Unlike prior 3D Gaussian Splatting (3DGS) methods that store view-dependent color and opacity for each Gaussian, VEG decouple the visual appearance from the data representation by encoding only scalar values, enabling transfer-function-agnostic rendering of 3DGS models for interactive scientific visualization. VEG are directly initialized from volume datasets, eliminating the need for structure-from-motion pipelines like COLMAP. To ensure complete scalar field coverage, we introduce an opacity-guided training strategy, using differentiable rendering with multiple transfer functions to optimize our data representation. This allows VEG to preserve fine features across a dataset’s full scalar range while remaining independent of any specific transfer function. Each Gaussian is scaled and rotated to adapt to local geometry, allowing for efficient representation of unstructured meshes without storing mesh connectivity and while using far fewer primitives. Across a diverse set of data, VEG achieve high reconstruction quality, compress large volume datasets by up to  $3600\times$ , and support lightning-fast rendering on commodity GPUs, enabling interactive visualization of large-scale structured and unstructured volumes.

**Index Terms**—Volume Rendering, Gaussian Splatting, Compression

## 1 INTRODUCTION

As high-performance computing (HPC) systems continue to grow in scale, scientific simulations are generating ever-larger and more complex datasets. These simulations frequently use adaptive mesh refinement (AMR) [1–3, 5, 6, 13] or unstructured meshes [1, 7, 24, 25] to efficiently represent physical phenomena. However, visualizing such massive volumes remains a significant challenge: datasets often exceed GPU memory, and visualization itself may require HPC resources, limiting interactivity and accessibility.

To address these challenges, recent work has explored machine learning (ML) representations for volume visualization [15, 43, 45, 46], offering promising methods for data compression and interactive rendering. However, prior ML-based techniques focus on regular grid data and struggle to generalize to the irregular geometry and explicit connectivity of AMR or unstructured meshes. This leaves a critical gap

in support for many real-world scientific datasets.

At the same time, 3D Gaussian Splatting (3DGS) has emerged as a powerful technique for real-time rendering of radiance fields, and has enjoyed an explosion of follow-up work since its initial debut [8, 11]. In 3DGS, a scene is represented by a set of 3D Gaussians, each defined by a position, scale, rotation, view-dependent color, and opacity. These Gaussians are projected into screen space and alpha-blended to form the final image. Each Gaussian’s parameters are optimized by an ML framework using differentiable rendering, and the training pipeline may dynamically densify or prune the total number of Gaussians. Once optimized, 3DGS techniques enable fast and high-quality rendering of real-world scenes.

However, 3DGS is fundamentally designed for surface-based, photogrammetry-derived datasets, not scientific volumes. Existing methods rely on structure-from-motion pipelines (e.g. COLMAP) to generate point cloud representations of real-world scenes, and they embed view-dependent color and opacity directly into each Gaussian. This makes them incompatible with the dynamic transfer function workflows that are typically applied to volume visualization. To be useful

\*Both authors contributed equally to the paper.

for scientific exploration, users must be able to adjust color and opacity mappings interactively, which standard 3DGS representations cannot support.

To address this gap, we present *Volume Encoding Gaussians (VEG)*, a novel 3DGS representation tailored for scientific volume visualization. Rather than storing color and opacity for each Gaussian, VEG store only scalar field values, decoupling the data representation from its visual properties. This allows VEG to support transfer-function-agnostic rendering, where arbitrary color and opacity mappings can be applied dynamically at render time. Because of their 3D Gaussian representation, VEG can model complex geometry accurately by scaling and rotating to align with local structures, without storing expensive mesh data about AMR or unstructured connectivity. Additionally, each Gaussian can cover a large spatial region, so VEG requires far fewer primitives than the number of original volume cells, improving both storage and rendering efficiency.

To ensure that VEG capture the full function range of a given dataset, we introduce an opacity-guided training strategy. During training, the model is optimized against ground-truth renderings produced using multiple transfer functions, each highlighting different data ranges. This encourages the Gaussians to accurately represent the entire scalar field. The result is a high-quality, compressed representation of the original volume dataset that preserves spatial features while offering interactive volume rendering performance.

Our work presents the following contributions:

- A high-quality, compressed representation (VEG) for structured and unstructured volume data using 3D Gaussians, enabling real-time rendering of large volumes with arbitrary transfer functions.
- A direct initialization pipeline from volume data, eliminating the need for structure-from-motion scene reconstruction tools.
- An opacity-guided multi-transfer-function training strategy, ensuring accurate reconstruction across an entire scalar field.
- A comprehensive evaluation demonstrating that VEG achieves high reconstruction quality, extreme compression (up to 1800 $\times$ ), and interactive visualization on large-scale scientific volumes.

## 2 RELATED WORK

Rendering of large-scale AMR and unstructured volumes is a long-studied problem in scientific visualization, and is required as part of our training pipeline. In [Section 2.1](#), we briefly review relevant recent work on volume rendering techniques. As neural networks can be sampled quickly and represent volume data without scaling linearly with dataset size, they offer a compressed data representation that can be used for efficient rendering. While our work does not produce a neural representation, it is similar to methods that do in that we use machine learning to optimize our VEG to represent volume data. Because of this, we review neural representations for compressing and rendering volume data in [Section 2.2](#). Finally, since our work draws heavily from 3D Gaussian splatting, we will give a brief background for this work in [Section 2.3](#).

### 2.1 Direct Volume Rendering of Large Datasets

Interactive direct volume rendering of AMR and unstructured volumes has long been a focus area in visualization [4, 29, 33, 42]. Ever larger data sets and the desire for faster rendering or higher visual quality pose a continuous challenge, while new hardware capabilities provide opportunities for new techniques [19–21, 27, 28]. Here we briefly review recent work for background, and refer the reader to the excellent survey by Sarton et al. [29] for more details.

Work on volume rendering has roughly converged on ray tracing as the fundamental primitive for traversing and integrating the volume to produce a color for each pixel [19–21, 27–29, 38]. Recent work has focused on leveraging GPU ray tracing hardware to accelerate ray traversal and space skipping [19–21, 28, 38]. As the GPU does not provide native support for AMR or unstructured elements, prior work has constructed various forms of spatial hierarchies over the data to produce a partitioning that a GPU bounding volume hierarchy can be

constructed over to leverage the hardware. For example, these spatial partitions can be bricks [38], shells [28] or clusters [19]. Additional metadata about the volume value ranges in a partition can also be stored and used to accelerate traversal [19, 20, 38]. We use PyVista [35] to produce ground truth images and samples in our training pipeline; however, it can struggle even on medium size volumes. Integrating recent work on GPU-accelerated rendering and sampling would greatly improve the scalability of our training pipeline.

### 2.2 Neural Representations for Volume Data

As huge advances have been made in deep learning, these techniques have naturally been applied for scientific visualization. While there has been much work in this field (see the recent survey by Wang and Han [39]), here we will focus on papers that use machine learning for compression and reconstruction of volume data. Weiss et al. [44] showed the possibility of reconstructing volume data from ground truth images using differentiable rendering, a method which we employ in our work. Jain et al. [10] presented a neural method for compressed volume rendering of multivariate time-varying volumes. Kim et al. created NeuralVDB [12], which uses neural networks to further improve the compression ability of the VDB [23] data structure for sparse volumes. Due to the size of the respective fields, there is a recent trend in volume visualization for state-of-the-art methods to adapt groundbreaking work in computer vision to representing volume data, with large success. Lu et al. created *Neurcomp* [15], which adapts SIREN’s [34] implicit neural representation for efficient volume data compression. Weiss et al. took inspiration from this with fV-SRN [43], which uses dense-grid encoding [37] and fast tensor core inference to build a neural representation that supports interactive rendering. Wu et al. then greatly improved on fV-SRN’s performance (in terms of reconstruction quality, training time, and rendering speed) with InstantVNR [46], which uses multi-resolution hash encoding [22] for its neural representation, and extends it with out-of-core training and batch inference during volume rendering. We hope to continue this trend by adapting the use of 3D Gaussians to represent volume data. Importantly, our work is the first to specifically address unstructured volumes, as the related work has so far focused solely on building representations for structured data. In addition, we uniquely explore the possibility of learning an explicit point-based representation for building a model of volume data.

### 2.3 3D Gaussian Splatting

Splatting methods involve projecting a set of 3-dimensional primitives directly onto a 2-dimensional image, then  $\alpha$ -blending the primitives in order of their depth. Zwicker et al. [48] first proposed the use of Gaussian filters as a primitive for splatting, showing their effectiveness for rendering both surface and volume data. Kerbl and Kopanas et al. [11] noted that, while the rendering algorithm for Gaussian splatting is very different, its image formation model is essentially the same as traditional volume rendering methods such as those in neural radiance field rendering (NeRF) [18], allowing for accurate scene representation. At the same time, the explicit nature of 3D Gaussians allows for fast rendering compared to the expensive sampling necessary for rendering with the continuous implicit neural representation of NeRFs.

Originally developed for photogrammetry-based scene reconstruction, in 3DGS each Gaussian stores an opacity along with view-dependent color using spherical harmonics, similar to previous work [9, 22]. In addition, initializing a set of 3D Gaussians relies on point clouds derived from NeRFs, COLMAP [30, 31] or similar structure-from-motion pipelines. These features of 3DGS are inherently designed for real-world image datasets, making them unsuitable for scientific volume data. Visualization of scientific volumes commonly uses direct volume rendering [16] techniques, where scalar field values are mapped to optical properties using transfer functions consisting of color and opacity maps. Arbitrary transfer functions are needed for data exploration, to enable flexible visualization of different features within the volume. Unlike scene reconstruction, volume rendering must support interactive transfer function adjustments, meaning that embedding color into the data representation is impossible. In our work, we address this through our development of Volume Encoding Gaussians which

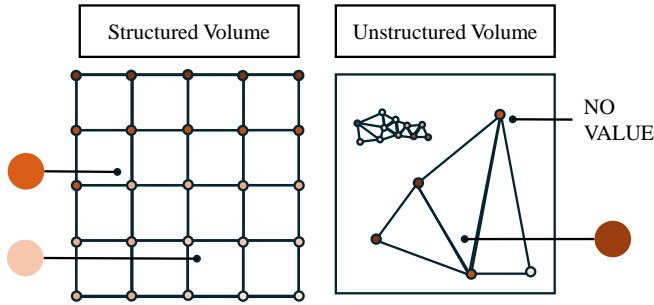


Fig. 2: Visualization of sampling for structured (left) and unstructured (right) volumes. Structured volumes define scalar fields over a regular grid, while unstructured volumes must define an explicit geometry that may have non-uniform spacing.

represent the underlying data field of a volume directly. Moreover, we replace the use of scene reconstruction for initializing our 3D Gaussians, instead directly using the given volume dataset.

### 3 DESIGN OF VEG

In this section we describe VEG, an extension of 3DGS that is tailored to scientific volume visualization.

#### 3.1 Volume Types

A structured volume is defined by a set of scalar field values on a regular grid, with neighboring points assumed to be connected grid cells. The geometry of a structured grid is defined implicitly; only the data values need to be stored since the grid dimensions and spacing are known a priori. Any point in space can be interpolated directly from the surrounding grid points, as shown in Figure 2. In contrast, unstructured volume data requires explicit storage of the geometry over which the scalar field is defined. Given a position in space, a test is performed to determine what cell in the volume, if any, contains it, before interpolating between that cell’s vertices to find the scalar value at that position. An example of this is also shown in Figure 2.

#### 3.2 The VEG Representation

Both structured and unstructured volume data can be defined as functions that map positions in a subset of 3-dimensional space to values in a scalar field, i.e.  $\Phi : \Omega \subset \mathbb{R}^3 \rightarrow \mathbb{R}, (x, y, z) \mapsto \Phi(x, y, z) = v$ . They differ in that, while the domain of a structured volumetric function is easily defined in space by its origin and bounds, the domain of an unstructured volumetric function has no set structure; the function can be defined over a completely arbitrary region matching the unstructured volume’s geometry. In addition, the complexity of this function is not uniform with respect to spatial area, as values in an unstructured volume can have arbitrary spacing. In practice, efficient representation of scalar fields with massive differences in spatial feature density is the main reason for using unstructured volumes.

Current neural representations for structured volume data [15, 43, 46] utilize scene representation networks [17, 18, 26], which implicitly model a volumetric function from input positions to scalar values using neural networks. Because of the unique features of unstructured volumetric functions mentioned above, the extension of neural methods to unstructured volume data is not readily apparent. In our work, we instead propose an explicit, point-based representation of unstructured volumes in order to encode both the volume’s geometry and underlying scalar field.

To do this, we use a 3D Gaussian formulation [11], where each point is defined as an ellipsoid centered at position  $\mu$  with 3-dimensional scaling and rotation matrices,  $S$  and  $R$ . This allows the points to translate, stretch, and rotate independently in each dimension, giving the representation freedom to adapt to the arbitrary geometries of unstructured volumes. In addition, each Gaussian stores a value, allowing it to record the scalar field over the covered area of the unstructured volume’s geometry. In this way, our Volume Encoding Gaussians (VEG)

give a compact representation that can encode the full information of an unstructured volume. While unstructured volumes are made up of both scalar-valued points and the connectivity information describing the cells connecting those points, the geometry-capturing nature of 3D Gaussians allows our representation to be simply made up of scalar-valued Gaussians, without storing any connectivity information.

### 4 DIFFERENTIABLE RENDERING OF VEG

The goal of our representation is to approximate direct volume rendering [16] of the ground truth dataset. Specifically, we target simple raymarching with the emission-absorption model, where the color of each pixel is given by accumulating the contribution of  $N$  samples along the ray using  $\alpha$ -blending with the discretized equation:

$$C = \sum_{i=0}^N c_i \cdot \alpha_i \cdot \prod_{j=0}^{i-1} (1 - \alpha_j) \quad (1)$$

A given transfer function is used to map samples  $i$  of the represented scalar field to opacity  $\alpha_i$  (emission) and color  $c_i$  (absorption). For our algorithm, rather than evaluating a transfer function when accumulating samples, it is more efficient to apply the transfer function as the first step of our rendering algorithm, converting the attached scalar value of each Gaussian to an opacity and color. This allows us to immediately cull Gaussians with values mapped to very low opacities, saving computation time analogously to empty space skipping in traditional volume rendering.

After the transfer function has been applied, we use 3D Gaussian splatting to model Equation 1 exactly. To render each Gaussian, the scaling and rotation matrices are used to create the Gaussians’ 3-dimensional covariance matrix, which is then projected to a 2-dimensional covariance matrix using the method of Zwicker et al. [48]. This converts the 3D Gaussian in object space into a 2D Gaussian in image space. The list of 2D Gaussians intersecting the screen can then be used to create the rendered image using the efficient tile-based rasterizer of Kerbl and Kopanas et al. [11]. This rasterizer employs  $\alpha$ -blending of splatted Gaussians in front-to-back order, where a pixel accumulates transfer function-determined color from each Gaussian intersecting it by evaluating its 2D covariance matrix (using the method of Yifan et al. [47]) multiplied by the opacity given to it by the transfer function. This solves Equation 1, effectively approximating the emission-absorption model for raymarching-based volume rendering.

For the backwards pass of rendering, gradients are computed manually for each Gaussian parameter using a modified version of Kerbl and Kopanas et al.’s [11] rasterizer. In order to optimize the attached scalar values for each Gaussian, we backpropagate gradients with respect to color and opacity through the transfer function used to render that frame. We assume linear interpolation of color and opacity between each control point of the given transfer function, but allow for an arbitrary number of control points to be given. To constrain values within  $[0, 1)$  and ensure smooth gradients during training, we utilize a sigmoid activation function for storing scalar values.

### 5 OPTIMIZATION OF VEG

The essence of our method is our optimization of Volume Encoding Gaussians to accurately represent an unstructured volume. In this section, we will outline our strategy, starting with how we initialize our data representation in Section 5.1. We will then detail our method for training the representation from this starting point to completion in Section 5.2.

#### 5.1 Initialization

As shown in previous work [11], proper initialization is incredibly important for learning explicit scene representations. Because the input to our method is a volume dataset, it is important to initialize our VEG with some knowledge of the scalar field it will be trained to represent.

To do this, we experimented with initializing VEG from either cell centers or vertices of the volume. Most commonly, volume data is stored with values defining its scalar field attached to points in space, which are then connected as vertices of cells. In order to initialize our

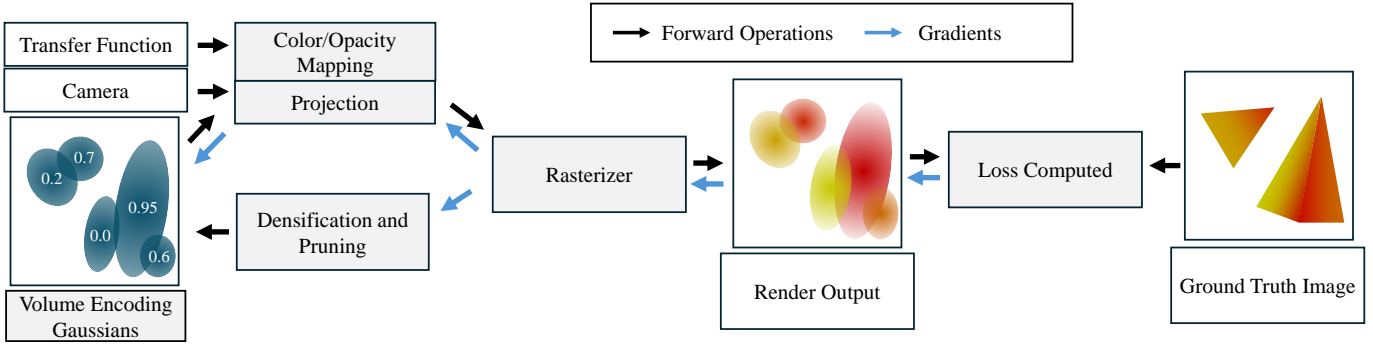


Fig. 3: Diagram of our training pipeline, where operation flow is depicted with black arrows and gradient backpropagation is depicted with blue. We conduct image-space training, in which our differentiable rendering algorithm is used to optimize Volume Encoding Gaussians from loss computed against ground truth images. Each training step, we render our VEG by opacity/color mapping with a given transfer function, projection into 2D with a given camera view, then rasterization and blending of the 2D colored primitives. We then compare the rendered output against reference images created from volume rendering with an emission-absorption model. After computing loss, gradients are backpropagated through to the scaling, rotation, position, and scalar values of the VEG for optimization. Gradients are also used for densification and pruning of the VEG, in which the density of 3D Gaussians in space is adaptively controlled.

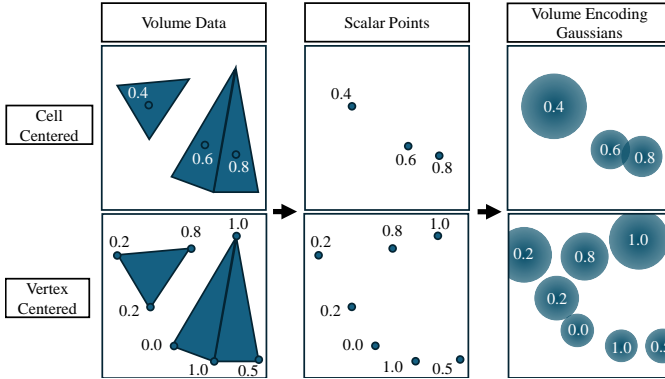


Fig. 4: Diagram of our initialization strategy to create Volume Encoding Gaussians from input volume data. For both cell-centered and vertex-centered data, our approach begins by deleting all connectivity information, leaving only scalar-valued data points in space. Next, we extend these data points with 3D scaling and rotation matrices, so that each point is now a 3D Gaussian with attached data value. These matrices are initialized to make each initial 3D Gaussian a sphere with size relative to the density of other points around it, with lower density creating larger Gaussians.

VEG, we first drop the connectivity information, and treat the scalar-valued vertices as a point cloud with each point storing a value. In our cell-centered initialization, we first interpolate the value of the scalar field for the center of each cell in the volume, then again drop the connectivity information and obtain a point cloud of scalar-valued cell centers. From either cell-centered or vertex-centered point cloud, we then transform each point into a VEG centered at the same position with the same scalar value in order to create our starting representation. We initialize each VEG as a scaled sphere depending on the proximity of its closest neighbors, with larger Gaussians in areas of empty space and smaller Gaussians in areas of high density. This process is shown for both cell-centered and vertex-centered initialization in Figure 4. We found both methods of initialization to give around equal performance; in our evaluation, we use vertex-centered initialization.

After initialization, the first step of our training process is to randomly drop away a percentage of the set of VEG, as the volume is typically heavily over-reconstructed with all points stored. We observe that the percentage of Gaussians dropped out here can significantly affect the final compression ratio and reconstruction quality, with the optimal value depending on data size and complexity. We explore how different dropout percentages affect training for different datasets in

## Section 6.

### 5.2 Training

To optimize our Volume Encoding Gaussians, we conduct image-space training using our fast differentiable rendering algorithm described in Section 4. Our complete training pipeline is shown in Figure 3. The Gaussian model is iteratively optimized to match training images, updating Gaussians’ position, scale, rotation, and scalar values. Through this, the VEG are able to learn both the geometry of the volume and value of the scalar field.

In order for our representation to accurately recreate a volumetric dataset, the model must have training data that can allow it to learn all of the dataset’s information. This process requires creating a training set of images with corresponding transfer functions and camera information used for rendering. We accomplish this by rendering a set of ground truth images using PyVista’s [35] VTK backend [32] for raymarching volumes with an emission-absorption model. Images are rendered in a full camera orbit to ensure complete coverage of the given dataset. After optimization, this allows the model to infer images of camera angles never seen during training.

Importantly, our model must also be able to render images for transfer functions never seen during training. This requires careful reconstruction of the full function range of the dataset. For this, the choice of transfer functions used to create the training set of images is incredibly important. Because optimization is done from loss computed between rendered images, transfer functions which highlight different ranges of the scalar field effectively weight the set of VEG to reconstructing the regions of the dataset containing those highlighted ranges. We found that, while the mapping of values to color does somewhat affect the resulting trained VEG, opacity mapping was especially significant to deciding which areas of the volume were reconstructed. This makes sense intuitively, since areas of value mapped to high opacity will be rendered with high opacity in resulting images, making them more impactful on image-based loss, which leads optimization to assign more relevance towards reducing their error.

We take advantage of this to improve the reconstruction quality of our models with *opacity-guided training*, where we use the opacity applied by transfer functions as an importance mapping to reconstruct all areas of the given dataset. To create our training set of images, we render each camera angle with multiple opacity maps highlighting different areas of the scalar field’s range. We design these opacity maps so that, in combination, every area of the range is weighted as equally important. Because these opacity maps will be used for optimizing the scalar values of our VEG, it is also important that the mapping between value and opacity in each has slope, in order for gradients to move values up or down during training. We build the set of opacity maps by first dividing the function range into a number of

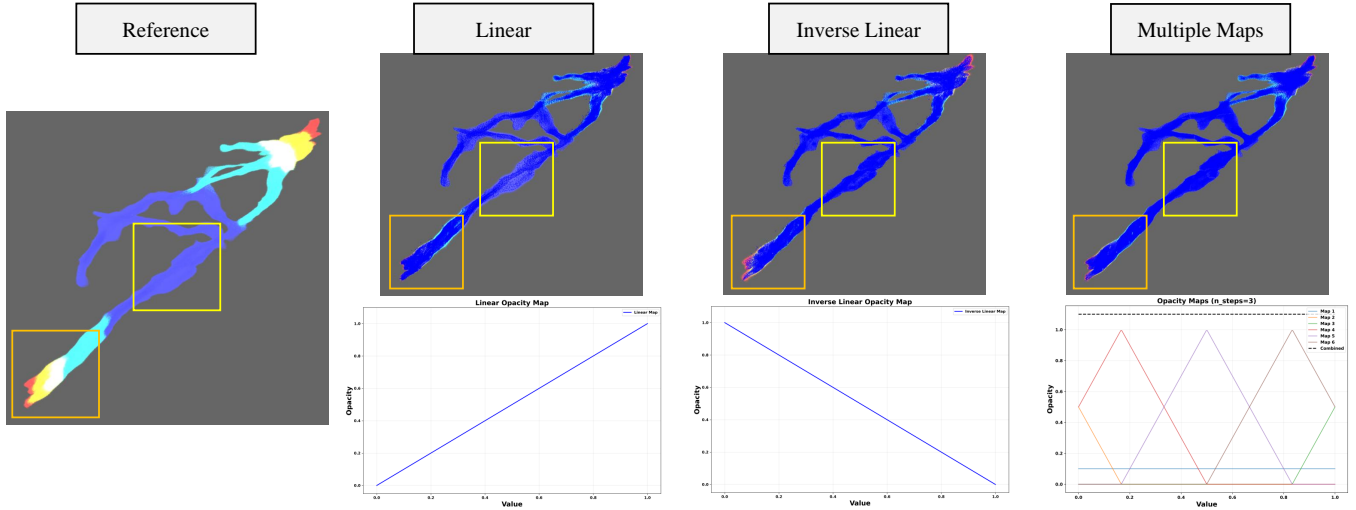


Fig. 5: Gaussian density comparison of VEG models trained using either a linear opacity map, an inverse linear opacity map, or our multiple opacity map method using three steps on the RBL dataset. Reference shows volume rendering with a pale rainbow colormap, where high values are red and low values are pale blue. Gaussian centers are painted using deep blue for each of the trained models, on top of the reference image, using SuperSplat’s [36] 3D Gaussian editor. Selected areas of high value are highlighted with an orange box, and areas of low value are highlighted with a yellow box. Notice how the model trained with the linear transfer function (which gives high opacity to high values) leads to greater Gaussian density in areas of high values and very low density in areas of low values, while the model trained with the inverse linear map does the opposite. Our multiple opacity map method leads to equal density for both areas of the function range.

steps, which we take as an input parameter. We then create an opacity map centered in each step, with linear drop-off around this center having slope equal to the number of steps. To ensure the lowest and highest values in the dataset are also weighed equally, two more maps are created just focused on those sets of values. We explore the number of steps necessary for effective training in Section 6. We observe that our approach improves the accuracy of VEG for reconstructing high frequency features of datasets. To ensure that low frequency features are modeled and the entire domain of the volume will be filled with Gaussians, we additionally include a single constant opacity map in our training set. A visual comparison of trained Gaussian density resulting from our opacity-guided training technique against naive approaches is given in Figure 5.

Depending on the scalar-value range of a given dataset, these opacity maps may yield entirely black images in the ground truth renders. For example, the Pig Heart dataset is mostly empty for about half of its function range, resulting in blank images for certain opacity maps highlighting this range. The inclusion of these blank images during training was found to significantly degrade the reconstruction quality of the VEG models. To mitigate this, each ground-truth image is evaluated and excluded from the training set when it is found to be too empty to contain enough information for training.

For each training iteration, a random camera angle and transfer function are chosen from the training set. The current set of VEG are then rendered and compared against the ground truth image for the same parameters in order to compute loss. We compute loss using the following equation:

$$\mathcal{L} = (1 - \lambda)\mathcal{L}_1 + \lambda\mathcal{L}_{MSSIM} + \mathcal{L}_{Scaling} + \mathcal{L}_{Bounding} \quad (2)$$

$\mathcal{L}_1$  and  $\mathcal{L}_{MSSIM}$  are L1 and MSSSIM [40, 41] loss computed between the render and ground truth, and  $\lambda$  is a parameter weighing them against each other. We set  $\lambda$  to 0.55 for all our tests.  $\mathcal{L}_{Scaling}$  is a small additional loss term defined as:

$$\frac{1}{N} \sum_{i=1}^N \left\| \frac{1}{S_i} \right\|_2 \quad (3)$$

where  $S_i$  is the scaling matrix of Gaussian  $i$ . This term takes the mean of the L2 norms for the inverted scaling of each Gaussian. This effectively penalizes Gaussians from becoming smaller, promoting

them to represent the unstructured volume with fewer, larger Gaussians when possible to save memory and computation. The choice of  $\lambda_{scaling}$  can affect compression factor and reconstruction quality, as increasing its value can reduce the number of Gaussians in the representation but also lead to under-reconstruction of high frequency features. We set our default value of  $\lambda_{scaling}$  to  $1e^{-5}$  based on initial tests and explore using different values in Section 6. Additionally, we add another loss term  $\mathcal{L}_{Bounding}$  defined as:

$$\frac{1}{N} \sum_{i=1}^N \sum_{d \in \{x,y,z\}} \left( \max(\mu_{i,d} - b_d^{\max}, 0) + \max(b_d^{\min} - \mu_{i,d}, 0) \right)^2 \quad (4)$$

where  $b$  stores the bounding box (in terms of maximum and minimum  $x$ ,  $y$ , and  $z$ ) of the original volume being modeled. This loss helps to encourage the VEG to stay within the convex hull of the original dataset, preventing drift and maintaining consistency of coordinate position between the representation and original volume.

While optimization of our set of Gaussians enables them to represent volumes, for best results, training needs some way to adaptively control the density of Gaussians in space. This should allow for removing Gaussians from areas where they are unneeded, saving memory and computation, and adding them to areas where the current number of Gaussians cannot accurately represent the volume’s complexity. This is accomplished via densification and pruning heuristics during training. For densification, we follow the method of Kerbl and Kopanas et al. [11]. They show that, if a Gaussian has large view-space positional gradients, it is likely because it is in a region that is not well reconstructed. Therefore, new Gaussians need to be added to that area, which is done by either cloning or splitting the Gaussian with large gradient depending on its size. For pruning, while their work removes Gaussians with low attached opacity, our VEG do not store a per-gaussian opacity to use for destruction. Instead, we cull Gaussians if they fit one of two cases: either their gradient with respect to opacity is above a given threshold, meaning optimization would make them transparent if per-Gaussian opacities were stored, or their scaling has gone below a threshold, meaning they are too small to be relevant to rendering. We find that these heuristics are sufficient for keeping the number of Gaussians in a model in check and preventing exponential blowup from densification.

## 6 EVALUATION

Dataset	Dimensions	Dataset	Tetrahedra
Skull	(256, 256, 256)	Blunt Fin	0.22M
Magnetic	(512, 512, 512)	Jets	1.00M
Kingsnake	(1024, 1024, 795)	RBL	3.89M
Chameleon	(1024, 1024, 1080)	Corie	3.90M
Instability	(2048, 2048, 1920)	Mito	5.54M
Pig Heart	(2048, 2048, 2612)	SF1	13.98M

Table 1: Chosen datasets and their size. Separated into structured volumes (left) and unstructured volumes (right).

In this section, we perform an extensive evaluation of our method with regards to reconstruction quality, compression, training time, and rendering performance, and provide ablations of our major design decisions. We list our datasets and setup for each experiment in ???. Our first study is to benchmark the reconstruction quality of our method on every dataset while using a constant number of Gaussians, presented in Section 6.2. Next, we experiment with changing the dropout used for initialization of our models, showing that this allows our method to exchange some reconstruction quality for higher compression ratios in Section 6.3. Then, we perform an ablation study of the different design decisions of our method in Section 6.4. Finally, we present rendered output for all of our datasets along with performance in terms of FPS in Section 6.5.

### 6.1 Experimental Setup

**Datasets** We benchmark our method on 12 different datasets, consisting of 6 structured volumes from the Open SciVis Datasets [14] collection (Skull, Magnetic, Kingsnake, Chameleon, Instability, and Pig Heart) and 6 unstructured volumes used in previous work [27] (Blunt Fin, Jets, Mito, RBL, SF1, Corie). The datasets vary greatly in size, complexity, and structure, in order to showcase the potential of VEG across a variety of visualization scenarios, and stress-test the method’s ability to represent fine structures and large volumes. The structured volumes vary in dimensions from  $256^3$  (Skull) all the way to  $> 2048^3$  (Pig Heart), while the unstructured volumes vary in number of cells from 224,000 (Blunt Fin) to 13.98 million (SF1). The size of each dataset is given in Table 1.

**Training/System Setup** We trained each of our models for 30k iterations using images rendered at a resolution of  $512 \times 512$ . Unless otherwise noted,  $\lambda_{scaling}$  was set to  $1e^{-5}$  and 5 opacity map steps were used for training. All training and rendering benchmarks were conducted on a workstation with an AMD Ryzen Threadripper PRO 5975WX CPU, an NVIDIA RTX A6000 GPU (48GB VRAM), and 500GB of system RAM. While this amount of RAM allows us to load all of our datasets in memory, our trained models make up a fraction of the original datasets’ size and can be rendered even with lightweight laptops.

**Metrics** In order to evaluate our approach, we need to fairly compute metrics for reconstruction quality, compression, training time, and rendering performance. For reconstruction quality, we compare the output of our models to ground truth images on camera angles and transfer functions that were never used during training. We create 50 transfer functions with random opacity maps, where both the center and the slope of the opacity map are chosen randomly. Each transfer function is used to render 16 camera angles, and average SSIM and PSNR values are computed between the ground truths and images created by our models. For compression, we compare the size of the loaded datasets to the final size of our trained models. A limitation of our method currently is that the scalar values attached to our VEG must be type float32, even when the original dataset is a lower precision type. To account for this, all of the original datasets were resampled to float32 before being used as input to our system. For training time, we measure training while excluding the time to create ground truth images with PyVista, since our method could be used with any other rendering backend to create our training set. Finally, for rendering

300K Starting Gaussians Results					
Datasets	SSIM	PSNR	Size (MB)	Ratio	Time
Skull	0.948	31.09	13.49	4.76×	7.86
Magnetic	0.960	32.98	9.49	53.59×	7.73
Kingsnake	0.946	32.72	14.07	226.0×	7.71
Chameleon	0.964	31.81	12.88	335.4×	7.78
Instability	0.917	28.69	15.86	1936×	8.35
Pig Heart	0.985	41.89	11.53	3625×	7.74
Blunt Fin	0.986	37.29	3.28	2.87×	6.89
RBL	0.993	38.42	7.80	20.91×	9.58
Jets	0.922	29.86	8.37	4.97×	8.41
Corie	0.990	50.97	2.26	85.81×	10.76
Mito	0.978	32.83	12.88	17.96×	8.28
SF1	0.947	31.35	18.11	32.29×	9.69

Table 2: Results for VEG models trained from 300K random vertices chosen from the original volume. SSIM and PSNR are computed with respect to ground-truth images of the original datasets using cameras and transfer functions not seen during training. Results are separated into structured and unstructured volumes, and sorted by dataset size within each category. We observe that by setting a constant number of vertices to initialize the VEG from, we can limit training time (measured in minutes) and output size directly. Even for massive volumes (Instability, Pig Heart), we achieve a good approximation of the underlying dataset while drastically reducing size (compression ratios of 1936× and 3625×) and enabling extremely fast rendering.

performance, we simply take the average time of the render calls used for the image quality benchmarks, removing the first 20 iterations to account for warmup time.

### 6.2 Constant Dropout

We present benchmark results where each model was initialized from 300,000 randomly chosen vertices in Table 2. The model for each dataset still ends up with different sizes due to differences in densification and pruning during training. This study was done to evaluate the representative power of our VEG format, showing that even a relatively small number of starting Gaussians can achieve a good approximation of huge and complex datasets. Our results show we were able to achieve high image quality for unseen camera angles and random transfer functions for all models, while maintaining their memory footprint below 20MB and training time below 10 minutes. On small datasets, VEG achieved moderate compression, but large datasets saw extreme compression ratios while maintaining quality. This is largely due to VEG’s design, which stores fewer, spatially larger Gaussians to represent sparse regions of the volume. The motivating use case for VEG is to enable scientists to produce lightweight representations of prohibitively large datasets such that they can be visualized on local compute resources. In this regard, our results are very promising and demonstrate that datasets on the order of 10 to 40 GB can be represented as a VEG model while using less than 20 MB of memory.

### 6.3 Varied Dropout

In addition to using an exact number of starting vertices to initialize our VEG, we can instead use a percentage dropout to delete some portion of the vertices in the original volume before creating Gaussians from them. Directly mapping all volume data vertices or cell centers to Gaussians preserves structural detail but often over-initializes the VEG model, resulting in high memory usage and long training times without much improvement in compression ratios. Dropouts that are too low though, can lead to high compression ratios at the cost of not faithfully reconstructing the original volume dataset. To assess this tradeoff, we tested various dropouts (0.99, 0.999, and 0.9999) for all of our datasets, and present results in Table 3 and Table 4. Our experiments demonstrate a clear trade-off: aggressive dropout values yield substantial improvements to data compression and training times, although at a cost to image quality in the resulting model.

Varied Dropout Results - Structured						
Dataset	Dropout	SSIM	PSNR	Size	Ratio	Time
Skull	0.99	0.951	32.20	9.49	6.76×	8.20
	0.999	0.948	31.35	4.61	13.88×	7.70
	0.9999	0.950	31.25	4.02	15.96×	7.48
Magne.	0.99	0.955	32.91	17.30	29.59×	11.91
	0.999	0.964	33.93	7.46	68.60×	8.03
	0.9999	0.953	32.10	4.92	104.2×	7.65
Kings.	0.99	0.943	34.85	258.6	6.14×	55.01
	0.999	0.954	34.40	33.45	47.54×	11.49
	0.9999	0.943	31.90	6.10	260.5×	7.48
Chame.	0.99	0.970	34.20	212.7	20.24×	58.40
	0.999	0.957	33.38	33.25	129.9×	12.48
	0.9999	0.966	32.32	7.04	613.8×	7.87
Insta.	0.99	OOM	OOM	OOM	OOM	OOM
	0.999	0.914	29.20	137.0	224.2×	42.75
	0.9999	0.906	28.20	25.91	1185×	11.38
Pig H.	0.99	OOM	OOM	OOM	OOM	OOM
	0.999	0.970	40.05	240.3	173.9×	59.21
	0.9999	0.987	40.82	34.71	1204×	12.34

Table 3: Results for VEG models trained from the vertices of structured volumes at various dropouts. A dropout of 0.99 means 99% of vertices are deleted before initialization. Size is measured in MB, ratio is compression ratio, and time is measured in minutes. OOM indicates that the training pipeline crashed due to a CUDA out-of-memory error.

Overall, these results show that our method offers a compressive representation for both structured and unstructured volume data with high image quality. Comparing to the benchmarks of the state-of-the-art in neural representations for structured volumes [46], they achieve compression factors of 67×, 158×, 612×, and 6640× with PSNRs of 41.9, 54.3, 31.6, and 55.0 on the Skull, Chameleon, Instability, and Pig Heart datasets respectively. While our reconstruction quality metrics are less than theirs, the comparison is not direct due to their metrics being computed between their representation and volume directly, while ours is computed between output rendered with arbitrary transfer functions. Still, optimization is clearly needed if we are to match the quality of their approach when it comes to reconstruction quality vs. compression ratio on structured volumes.

Excitingly, though, we prove that our method can uniquely achieve a compressed ML-based representation for unstructured volumes. The compression afforded by our method varies heavily depending on the size and complexity of the dataset, with simpler datasets (RBL, Corie) and large datasets (Mito) able to achieve large compression ratios (> 70×) while maintaining high image reconstruction quality (PSNR > 32).

#### 6.4 Ablation Study

In this section, we conduct several tests for validation of design decisions made in the creation of Volume Encoding Gaussians. Specifically, we test the effect of our initialization strategy, our use of multiple opacity maps, our additional bounding and scaling loss terms, and our training of scalar values per Gaussian. To do this, we train models starting from 300k randomly selected vertices for 2 unstructured (Blunt Fin and RBL) and 2 structured (Skull and Magnetic) datasets, while changing various aspects of our algorithm. We present our results in Table 5. The "Defaults" row represents usage of the default parameters and method of our algorithm, and the metrics are taken directly from Table 2.

**Initialization** In conventional 3DGS, Gaussians are initialized with unit size and scale directly from COLMAP-generated point clouds. While random initialization is possible, and is the starting point when training on NeRF data, it typically results in poor convergence. To

Varied Dropout Results - Unstructured						
Dataset	Dropout	SSIM	PSNR	Size	Ratio	Time
Jets	0.99	0.921	28.18	4.07	10.38×	7.05
	0.999	0.943	30.49	3.96	10.65×	6.98
	0.9999	0.937	28.70	3.61	11.68×	6.90
RBL	0.99	0.993	37.2	1.16	146.8×	6.37
	0.999	0.994	37.7	1.45	117.6×	6.75
	0.9999	0.992	36.9	1.38	124.4×	6.94
Corie	0.99	OOM	OOM	OOM	OOM	OOM
	0.999	0.989	49.32	1.15	168.7×	7.06
	0.9999	0.989	46.65	1.15	168.6×	7.04
Mito	0.99	0.979	32.46	2.76	85.32×	6.20
	0.999	0.978	32.08	3.18	73.86×	6.43
	0.9999	0.965	26.44	4.95	46.73×	6.76
SF1	0.99	OOM	OOM	OOM	OOM	OOM
	0.999	0.955	29.70	24.29	24.04×	10.75
	0.9999	0.949	28.25	5.47	106.92×	7.25

Table 4: Results for VEG models trained from the vertices of unstructured volumes at various dropouts. A dropout of 0.99 means 99% of vertices are deleted before initialization. Size is measured in MB, ratio is compression ratio, and time is measured in minutes. The Blunt Fin dataset is excluded from this experiment since it is too small to be effectively trained with high dropout values. OOM indicates that the training pipeline crashed due to a CUDA out-of-memory error.

test our initialization strategy, we compared our default initialization against models trained from 300k points initialized with random centers and values. Similarly to 3DGS, we found that initializing VEG models randomly led to much worse reconstruction quality and spatial accuracy. This can be seen in the "Random Init" row of Table 5, which consistently had the lowest SSIM and PSNR values compared to all models initialized from volume data. This shows our initialization strategy is successful in providing a good starting point for VEG that allows the representation to accurately learn a given dataset.

**Multiple Opacity Maps** A key contribution of our work is our opacity-guided multiple-transfer-function training, in which we use multiple opacity maps to ensure that the entire function range of a volume is accurately represented. To test this, we compare training with our default 5 steps of opacity maps against naive training with a single linear opacity map. As can be seen in Table 5, our method is able to improve the image quality drastically for rendering arbitrary transfer functions; the PSNR of "Linear Opacity Map" ranges from 1.45 (for Skull) all the way to 5.73 (for Blunt Fin) behind our method. Interestingly, the naive method is able to achieve much better compression ratios, likely because areas of low value (mapped to low opacity in a linear transfer function) are under-reconstructed.

We also perform another experiment to gain insight into the number of opacity maps necessary for accurate volume reconstruction. We conduct training using our multiple opacity map method with number of steps varying from 1 to 6, and measure resulting image quality in the same way as other experiments. We show results for datasets Blunt Fin, RBL, Skull, and Magnetic in Figure 5. We observed diminishing returns in reconstruction quality (PSNR, SSIM) when training VEG models with more than one colormap or with more than 5 linearly ramped opacity maps. Conversely, VEG struggles to reconstruct finer structures when using fewer than 5 linearly ramped opacity maps.

**Additional Loss Terms** As mentioned in Section 5, besides our L1-MS\_SSIM image loss, we also use two additional loss terms computed directly on the set of VEG. The first is bounding loss, meant to ensure the 3D Gaussians in our representation remain in the same coordinate area as the given volume dataset. We test the usefulness of this feature with our "No Bounding Loss" test in Table 5. Surprisingly, we find that utilizing bounding loss during training has little improvement on image quality, with results nearly the same as our defaults. However, we did

	Blunt Fin			RBL			Skull			Magnetic		
	SSIM	PSNR	Ratio	SSIM	PSNR	Ratio	SSIM	PSNR	Ratio	SSIM	PSNR	Ratio
Random Init	0.745	16.44	0.52×	0.741	16.16	12.65×	0.912	24.89	4.28×	0.939	27.83	39.69×
Linear Opacity Map	0.962	31.56	3.02×	0.985	34.02	42.59×	0.920	29.64	5.6×	0.91	28.50	95.13×
No Bounding Loss	0.979	35.14	2.86×	0.993	38.13	20.9×	0.947	31.59	4.76×	0.961	32.85	54.27×
$\lambda_{scaling} = 0$	0.976	34.36	2.55×	0.991	36.46	13.11×	0.942	30.54	4.16×	0.954	33.06	30.12×
$\lambda_{scaling} = 5e^{-5}$	0.978	35.45	3.31×	0.992	36.98	25.34×	0.959	32.80	6.8×	0.947	31.22	75.61×
$\lambda_{scaling} = 2.5e^{-4}$	0.980	35.48	4.92×	0.992	36.78	66.79×	0.951	31.57	10.68×	0.940	30.51	102.72×
Interpolated Values	0.981	35.9	2.14×	0.994	38.09	24.41×	0.956	31.97	5.44×	0.941	30.45	65.12×
Defaults	0.986	37.29	2.87×	0.993	38.42	20.91×	0.948	31.09	4.76×	0.960	32.98	53.59×

Table 5: Ablation study comparing our defaults to various settings for training. Result metrics are image quality in the form of SSIM and PSNR, along with compression ratio. Best results for each dataset and metric are shown in red, second best are in orange, and third best are in yellow. Our defaults are usually the best performing when it comes to reconstruction quality. See Section 6.4 for more information about each of these tests.

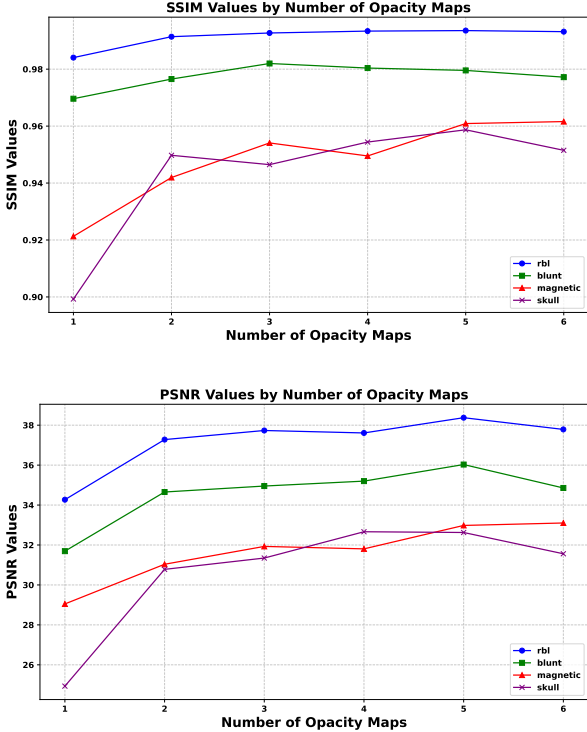


Fig. 6: Comparison of reconstruction quality as a function of number of opacity maps used for training. Two structured datasets (skull and magnetic) along with two unstructured datasets (blunt and RBL) were evaluated. Left: SSIM values. Right: PSNR values. Note that image quality increases heavily from a single opacity map to two, then rises slowly before reaching best performance at 5 opacity maps.

find through manual testing that our bounding loss term is successful in keeping Gaussians within the convex hull of the original dataset. We suspect that if we were to compute object space comparisons between our VEG and the original volume, this term would likely improve quality, even though it does not improve rendering quality.

The second additional loss term we utilize is scaling loss, which penalizes Gaussians for being small in space. To evaluate this feature, we test different weights for this loss at values  $\lambda_{scaling} = [0, 1e^{-5}, 5e^{-5}, 2.5e^{-4}]$ , where  $1e^{-5}$  is the default. Results shown in Table 5 suggest that higher weights for the scaling loss term effectively lead to higher compression ratios. This is due to this term optimizing VEG to become larger, meaning that fewer 3D Gaussians are needed to represent the full volume. However, we also find that increasing this term too much can result in lower image quality, as the Gaussians become so big that rendering output becomes blurry. We see this trend especially for complex datasets like Magnetic, where small Gaussians

are needed to represent high frequency features.

**Volume Value Training** Unlike 3DGS, which trains view-dependent color and opacity per Gaussian, VEG focus on reconstructing scalar volume fields. Each Gaussian is initialized with a value sampled from the volume, but as its position and shape change during training, this initial value will become invalid over time. In our default algorithm, this is remedied with optimization of each Gaussian’s attached value during training. In order to test the validity of this approach, we also implemented another strategy: interpolating values from the original volume whenever Gaussians significantly shift position. We show results for this approach as "Interpolated Values" in Table 5. We find that training values with gradient optimization leads to comparable image quality to interpolating values from the original volume. While training times are not shown in this comparison, we found training values to be much more memory efficient and quick to train due to avoiding interpolation overhead. Consequently, all other presented results utilize training of Gaussian scalar values.

## 6.5 Rendering

Finally, the last experiment we ran is to test the rendering performance for our trained models from Section 6.2. Notably, on the same system as we run benchmarks, all of our unstructured volumes except Blunt Fin can not be interactively explored with direct volume rendering, at least using popular renderers like PyVista and ParaView. In Figure 7, we present FPS and rendering results from applying random opacity maps with a rainbow colormap to our VEG representations. We do find very high variance in these result frame rates, likely because we only averaged frame time over a small number of iterations. Notably though, all of our models can be rendered with extremely high frame rates ( $> 200$ fps). In future work, we hope to evaluate this rendering performance on other systems, as we expect to maintain interactive performance even for extremely lightweight devices.

This experiment shows that VEG’s explicit representation supports incredibly fast rendering of our compressed data representation, allowing for exploration of large volumes on local compute resources. From previous experiments, we show that tunable training parameters can enable users to find the best balance between reconstruction quality and compression for their specific use case. VEG opens new possibilities for sharing, streaming, and rendering large-scale scientific datasets. Unlike traditional 3DGS, VEG decouples the data representation from the rendered visual appearance of the model, enabling accurate and real-time application of arbitrary transfer functions without reprocessing or retraining the model, but with the rendering performance of 3DGS.

## 7 CONCLUSION

In this paper, we introduced *Volume Encoding Gaussians (VEG)*, a novel 3D Gaussian splatting (3DGS) approach tailored specifically for structured and unstructured scientific volume rendering. VEG departs from conventional 3DGS primarily by removing view-dependent color and opacity encodings and instead directly encoding scalar-value fields from volume datasets. This effectively decouples the visual appearance from data representation, enabling highly compressed, lightweight,

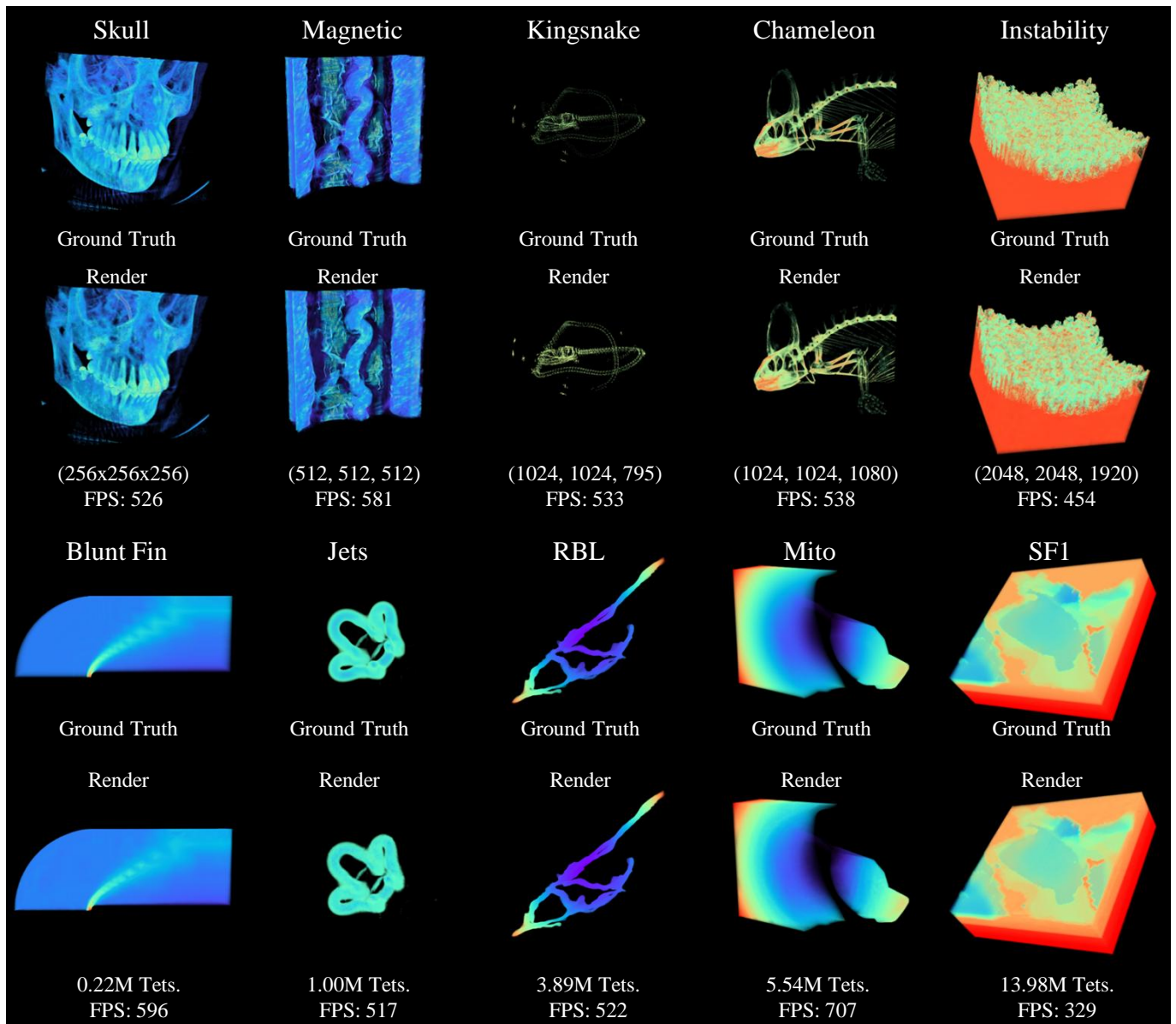


Fig. 7: Ground truth (top) and rendered images from our Table 2 models (bottom) using rainbow colormaps with random opacity functions. Our method renders accurate approximations of large structured (first row) and unstructured (second row) datasets while maintaining incredibly high FPS.

and transfer-function-agnostic reconstructions suitable for interactive visualization.

Our evaluation demonstrated that VEG achieves substantial compression, often several orders of magnitude, particularly beneficial for large datasets. Results showed excellent scalability, high reconstruction quality, and robust generalization to previously unseen transfer functions. Compared to existing volume compression techniques, VEG is able to accurately model complex scientific datasets while offering competitive compression ratios and leveraging the performance benefits of 3DGS for incredibly fast visualization. Remarkably, our work is the first to show the possibility for extending ML-based interactive representations to unstructured volumes.

We have several plans for extending and refining this work in the future. First, our current pipeline relies on PyVista for rendering ground-truth images of datasets. PyVista was selected over native VTK or a custom unstructured volume renderer to accelerate early development. However, PyVista struggles with performance, particularly for large unstructured volumes, and lags behind the latest versions of VTK. Transitioning directly to VTK or developing a custom renderer optimized

for unstructured data would substantially improve the robustness of our training process.

Second, while existing 3DGS renderers are incredibly full-featured, our approach requires post-processing to convert trained models into a compatible format for them. Because of this, existing interactive renderers are not capable of showcasing the full benefits of VEG. Developing a custom interactive renderer specifically tailored to VEG, capable of applying custom transfer functions dynamically, would greatly enhance the usability and effectiveness of our method for real-time scientific data exploration.

Finally, integrating recent advancements from the broader 3DGS community could yield additional performance improvements. Future work will explore lower-precision numeric representations (such as FP16 or quantization) for further reducing storage, support for time-varying volumetric data, and distributed training schemes to improve scalability for very large datasets and to enable training in HPC contexts.

## REFERENCES

- [1] W. K. Anderson, R. T. Biedron, J.-R. Carlson, J. M. Derlaga, B. Diskin, C. T. Druryor Jr, P. A. Gnoffo, D. P. Hammond, K. E. Jacobson, W. T. Jones, et al. Fun3d manual: 14.1. 2024. 1
- [2] D. Arndt, W. Bangerth, D. Davydov, T. Heister, L. Heltai, M. Kronbichler, M. Maier, J.-P. Pelteret, B. Turcksin, and D. Wells. The deal.II finite element library: Design, features, and insights. *Computers & Mathematics with Applications*, 2021. 1
- [3] M. Berger and P. Colella. Local adaptive mesh refinement for shock hydrodynamics. *Journal of Computational Physics*, 82(1):64–84, 1989. doi: 10.1016/0021-9991(89)90035-1 1
- [4] P. Bunyk, A. Kaufman, and C. T. Silva. Simple, Fast, and Robust Ray Casting of Irregular Grids. In *Scientific Visualization Conference (Dagstuhl '97)*, 1997. 2
- [5] C. Burstedde, L. C. Wilcox, and O. Ghattas. P4est : Scalable Algorithms for Parallel Adaptive Mesh Refinement on Forests of Octrees. *SIAM Journal on Scientific Computing*, 2011. 1
- [6] A. Dubey, K. Antypas, A. C. Calder, C. Daley, B. Fryxell, J. B. Gallagher, D. Q. Lamb, D. Lee, K. Olson, L. B. Reid, P. Rich, P. M. Ricker, K. M. Riley, R. Rosner, A. Siegel, N. T. Taylor, K. Weide, F. X. Timmes, N. Vladimirova, and J. ZuHone. Evolution of flash, a multi-physics scientific simulation code for high-performance computing. *The International Journal of High Performance Computing Applications*, 28(2):225–237, 2014. doi: 10.1177/1094342013505656 1
- [7] T. D. Economon, F. Palacios, S. R. Copeland, T. W. Lukaczyk, and J. J. Alonso. SU2: An Open-Source Suite for Multiphysics Simulation and Design. *AIAA Journal*, 2016. 1
- [8] B. Fei, J. Xu, R. Zhang, Q. Zhou, W. Yang, and Y. He. 3d gaussian splatting as new era: A survey. *IEEE Transactions on Visualization and Computer Graphics*, pp. 1–20, 2024. doi: 10.1109/TVCG.2024.3397828 1
- [9] Fridovich-Keil and Yu, M. Tancik, Q. Chen, B. Recht, and A. Kanazawa. Plenoxels: Radiance fields without neural networks. In *CVPR, 2022*. 2
- [10] W. Griffin, A. Godil, J. Bullard, J. Terrill, A. Varshney, and S. Jain. Compressed volume rendering using deep learning. Proceedings of the Large Scale Data Analysis and Visualization (LDAV) Symposium, Phoenix, AZ, 2017-10-02 2017. 2
- [11] B. Kerbl, G. Kopanas, T. Leimkuehler, and G. Drettakis. 3d gaussian splatting for real-time radiance field rendering. *ACM Trans. Graph.*, 42(4), article no. 139, 14 pages, July 2023. doi: 10.1145/3592433 1, 2, 3, 5
- [12] D. Kim, M. Lee, and K. Museth. Neuralvdb: High-resolution sparse volume representation using hierarchical neural networks. *ACM Trans. Graph.*, 43(2), article no. 20, 21 pages, Feb. 2024. doi: 10.1145/3641817 2
- [13] C. C. Kiris, J. A. Housman, M. F. Barad, C. Brehm, E. Sozer, and S. Moini-Yekta. Computational framework for launch, ascent, and vehicle aerodynamics (lava). *Aerospace Science and Technology*, 55:189–219, 2016. doi: 10.1016/j.ast.2016.05.008 1
- [14] P. Klacansky. Open scivis datasets, December 2017. <https://klacansky.com/open-scivis-datasets/>. 6
- [15] Y. Lu, K. Jiang, J. A. Levine, and M. Berger. Compressive neural representations of volumetric scalar fields. *Computer Graphics Forum*, 40(3):135–146, 2021. doi: 10.1111/cgf.14295 1, 2, 3
- [16] N. Max. Optical models for direct volume rendering. *IEEE Transactions on Visualization and Computer Graphics*, 1(2):99–108, June 1995. doi: 10.1109/2945.468400 2, 3
- [17] L. Mescheder, M. Oechsle, M. Niemeyer, S. Nowozin, and A. Geiger. Occupancy networks: Learning 3d reconstruction in function space. In *2019 IEEE/CVF Conference on Computer Vision and Pattern Recognition (CVPR)*, pp. 4455–4465, 2019. doi: 10.1109/CVPR.2019.00459 3
- [18] B. Mildenhall, P. P. Srinivasan, M. Tancik, J. T. Barron, R. Ramamoorthi, and R. Ng. Nerf: Representing scenes as neural radiance fields for view synthesis, 2020. 2, 3
- [19] N. Morrical, A. Sahistan, U. Gudukbay, I. Wald, and V. Pascucci. Quick clusters: A gpu-parallel partitioning for efficient path tracing of unstructured volumetric grids. *IEEE Transactions on Visualization and Computer Graphics*, 29(1):537–547, 2023. doi: 10.1109/TVCG.2022.3209418 2
- [20] N. Morrical, W. Usher, I. Wald, and V. Pascucci. Efficient Space Skipping and Adaptive Sampling of Unstructured Volumes Using Hardware Accelerated Ray Tracing. In *IEEE VIS Short Papers*, 2019. doi: 10.1109/VISUAL.2019.8933539 2
- [21] N. Morrical, I. Wald, W. Usher, and V. Pascucci. Accelerating Unstructured Mesh Point Location with RT Cores. *IEEE Transactions on Visualization and Computer Graphics*, 2020. doi: 10.1109/TVCG.2020.3042930 2
- [22] T. Muller, A. Evans, C. Schied, and A. Keller. Instant neural graphics primitives with a multiresolution hash encoding. *ACM Trans. Graph.*, 41(4), article no. 102, 15 pages, July 2022. doi: 10.1145/3528223.3530127 2
- [23] K. Museth. Vdb: High-resolution sparse volumes with dynamic topology. *ACM Trans. Graph.*, 32(3), article no. 27, 22 pages, July 2013. doi: 10.1145/2487228.2487235 2
- [24] N. Offermans, A. Peplinski, O. Marin, and P. Schlatter. Adaptive mesh refinement for steady flows in Nek5000. *Computers & Fluids*, 2020. doi: 10.1016/j.compfluid.2019.104352 1
- [25] F. Palacios, J. Alonso, K. Duraisamy, M. Colonna, J. Hicken, A. Aranake, A. Campos, S. Copeland, T. Economon, A. Lonkar, T. Lukaczyk, and T. Taylor. Stanford University Unstructured (SU<sup>2</sup>): An open-source integrated computational environment for multi-physics simulation and design. In *51st AIAA Aerospace Sciences Meeting Including the New Horizons Forum and Aerospace Exposition*. American Institute of Aeronautics and Astronautics, 2013. 1
- [26] J. J. Park, P. Florence, J. Straub, R. Newcombe, and S. Lovegrove. DeepSDF: Learning continuous signed distance functions for shape representation. In *2019 IEEE/CVF Conference on Computer Vision and Pattern Recognition (CVPR)*, pp. 165–174, 2019. doi: 10.1109/CVPR.2019.00025 3
- [27] B. Rathke, I. Wald, K. Chiu, and C. Brownlee. SIMD Parallel Ray Tracing of Homogeneous Polyhedral Grids. In *Eurographics Symposium on Parallel Graphics and Visualization*, 2015. doi: 10.2312/pgv.20151153 2, 6
- [28] A. Sahistan, S. Demirci, N. Morrical, S. Zellmann, A. Aman, I. Wald, and U. Gudukbay. Ray-traced Shell Traversal of Tetrahedral Meshes for Direct Volume Visualization. In *2021 IEEE Visualization Conference (VIS)*. IEEE, New Orleans, LA, USA, 2021. doi: 10.1109/VIS49827.2021.9623298 2
- [29] J. Sarton, S. Zellmann, S. Demirci, U. Gudukbay, W. Alexandre-Barff, L. Lucas, J. M. Dischler, S. Wesner, and I. Wald. State-of-the-art in Large-Scale Volume Visualization Beyond Structured Data. *Computer Graphics Forum*, 2023. doi: 10.1111/cgf.14857 2
- [30] J. L. Schonberger and J.-M. Frahm. Structure-from-motion revisited. In *Conference on Computer Vision and Pattern Recognition (CVPR)*, 2016. 2
- [31] J. L. Schonberger, E. Zheng, M. Pollefeys, and J.-M. Frahm. Pixelwise view selection for unstructured multi-view stereo. In *European Conference on Computer Vision (ECCV)*, 2016. 2
- [32] W. Schroeder, K. Martin, and B. Lorensen. *The Visualization Toolkit (4th ed.)*. Kitware, 2006. 4
- [33] C. Silva, J. Comba, S. Callahan, and F. Bernardon. A survey of GPU-Based volume rendering of unstructured grids. *Brazilian Journal of Theoretic and Applied Computing (RITA)*, 2005. 2
- [34] V. Sitzmann, J. N. P. Martel, A. W. Bergman, D. B. Lindell, and G. Wetzstein. Implicit neural representations with periodic activation functions, 2020. 2
- [35] C. B. Sullivan and A. Kaszynski. PyVista: 3d plotting and mesh analysis through a stream-lined interface for the visualization toolkit (VTK). *Journal of Open Source Software*, 4(37):1450, may 2019. doi: 10.21105/joss.01450 1, 2, 4
- [36] SuperSplat. <https://github.com/playcanvas/supersplat>. 5
- [37] T. Takikawa, J. Litalien, K. Yin, K. Kreis, C. Loop, D. Nowrouzezahrai, A. Jacobson, M. McGuire, and S. Fidler. Neural Geometric Level of Detail: Real-time Rendering with Implicit 3D Shapes. In *2021 IEEE/CVF Conference on Computer Vision and Pattern Recognition (CVPR)*, pp. 11353–11362. IEEE Computer Society, Los Alamitos, CA, USA, June 2021. doi: 10.1109/CVPR46437.2021.01120 2
- [38] I. Wald, S. Zellmann, W. Usher, N. Morrical, U. Lang, and V. Pascucci. Ray Tracing Structured AMR Data Using ExaBricks. *IEEE Transactions on Visualization and Computer Graphics*, 2021. doi: 10.1109/TVCG.2020.3030470 2
- [39] C. Wang and J. Han. DL4scivis: A state-of-the-art survey on deep learning for scientific visualization. *IEEE Transactions on Visualization and Computer Graphics*, 29(8):3714–3733, 20 pages, Aug. 2023. doi: 10.1109/TVCG.2022.3167896 2
- [40] Z. Wang, A. Bovik, H. Sheikh, and E. Simoncelli. Image quality assessment: from error visibility to structural similarity. *IEEE Transactions on Image Processing*, 13(4):600–612, 2004. doi: 10.1109/TIP.2003.819861 5
- [41] Z. Wang, E. Simoncelli, and A. Bovik. Multiscale structural similarity for image quality assessment. In *The Thirty-Seventh Asilomar Conference on Signals, Systems & Computers*, 2003, vol. 2, pp. 1398–1402 Vol.2, 2003. doi: 10.1109/ACSSC.2003.1292216 5
- [42] M. Weiler, M. Kraus, M. Merz, and T. Ertl. Hardware-based ray casting for tetrahedral meshes. In *IEEE Visualization*. IEEE Computer Society, 2003. doi: 10.1109/VISUAL.2003.1250390 2
- [43] S. Weiss, P. Hermuller, and R. Westermann. Fast neural representations for direct volume rendering. *Computer Graphics Forum*, 41(6):196–211, June 2022. doi: 10.1111/cgf.14578 1, 2, 3
- [44] S. Weiss and R. Westermann. Differentiable direct volume rendering. *IEEE Transactions on Visualization and Computer Graphics*, 28(1):562–572, 2022. doi: 10.1109/TVCG.2021.3114769 2
- [45] Q. Wu, D. Bauer, M. J. Doyle, and K.-L. Ma. Interactive Volume Visualization via Multi-Resolution Hash Encoding based Neural Representation. *IEEE Transactions on Visualization and Computer Graphics*, 2023. doi: 10.1109/TVCG.2023.3293121 1
- [46] Q. Wu, D. Bauer, M. J. Doyle, and K.-L. Ma. Interactive volume visualization via multi-resolution hash encoding based neural representation. *IEEE Transactions on*

*Visualization and Computer Graphics*, 30(8):5404–5418, 2024. doi: [10.1109/TVCG.2023.3293121](https://doi.org/10.1109/TVCG.2023.3293121) 1, 2, 3, 7

- [47] W. Yifan, F. Serena, S. Wu, C. Öztireli, and O. Sorkine-Hornung. Differentiable surface splatting for point-based geometry processing. *ACM Trans. Graph.*, 38(6), article no. 230, 14 pages, Nov. 2019. doi: [10.1145/3355089.3356513](https://doi.org/10.1145/3355089.3356513) 3
- [48] M. Zwicker, H. Pfister, J. van Baar, and M. Gross. Ewa volume splatting. In *Proceedings Visualization, 2001. VIS '01.*, pp. 29–538, 2001. doi: [10.1109/VISUAL.2001.964490](https://doi.org/10.1109/VISUAL.2001.964490) 2, 3